Journal of Computational and Applied Mathematics 235 (2011) 2740–2757

Contents lists available at ScienceDirect

Journal of Computational and Applied Mathematics

journal homepage: www.elsevier.com/locate/cam

A spectral-Galerkin continuation method using Chebyshev polynomials for the numerical solutions of the Gross–Pitaevskii equation

Y.-S. Wang [a], C.-S. Chien [b,*]

[a] Department of Applied Mathematics, National Chung Hsing University, Taichung 402, Taiwan

[b] Department of Computer Science and Information Engineering, Ching Yin University, Jungli 320, Taiwan

ARTICLE INFO

Article history:
Received 19 April 2010
Received in revised form 2 September 2010

Keywords:
Spectral methods
Bose–Einstein condensates
Symmetry-breaking solutions

ABSTRACT

We study an efficient spectral-Galerkin continuation method (SGCM) and two-grid centered difference approximations for the numerical solutions of the Gross–Pitaevskii equation (GPE), where the second kind Chebyshev polynomials are used as the basis functions for the trial function space. Some basic formulae for the SGCM are derived so that the eigenvalues of the associated linear eigenvalue problems can be easily computed. The SGCM is implemented to investigate the ground and first excited-state solutions of the GPE. Both the parabolic and quadruple-well trapping potentials are considered. We also study Bose–Einstein condensates (BEC) in optical lattices, where the periodic potential described by the sine or cosine functions is imposed on the GPE. Of particular interest here is the investigation of symmetry-breaking solutions. Sample numerical results are reported.

1. Introduction

Chebyshev polynomials have comprehensive applications in different branches of numerical analysis. One of the most important applications is in numerical partial differential equation [1–3]. Actually, there are four different kinds of Chebyshev polynomials [4]. Probably the most popular one is the first kind Chebyshev polynomials defined by $T_n(x) = \cos n\theta$ when $x = \cos\theta$; see e.g. [1,2,5,6]. In this paper, we will study spectral-Galerkin methods using the second kind Chebyshev polynomials [4] for the numerical solutions of the GPE

$$\begin{aligned} &\mathbf{i}\Psi_t(\mathbf{x},t) = -\Delta\Psi + \left[V(\mathbf{x}) + a\sin^2\left(\frac{\pi x}{d}\right) + b\sin^2\left(\frac{\pi y}{d}\right)\right]\Psi + \mu|\Psi|^2\Psi, \quad t > 0,\ \mathbf{x}\in\Omega,\\ &\Psi(\mathbf{x},t) = 0, \quad \mathbf{x}\in\partial\Omega,\ t\geq 0. \end{aligned} \tag{1.1}$$

Eq. (1.1) is also called a mean-field nonlinear Schrödinger equation (NLS) with local cubic nonlinearity. Here $\Psi(\mathbf{x},t)$ is the macroscopic wave function of the BEC, $V(\mathbf{x})$ the magnetic trapping potential, the coefficient μ can be positive or negative depending on the physical system is repulsive or attractive, a and b are positive constants, d is the distance between neighbor wells (lattice constant), and $\Omega \subset \mathbf{R}^n$, $n = 2, 3$, a bounded domain with piecewise smooth boundary $\partial\Omega$. The trapping potentials in (1.1) can be parabolic or quadruple-well, i.e.,

$$V(\mathbf{x}) = \frac{1}{2}(x^2+y^2), \quad \text{parabolic}, \tag{1.2}$$

$$V(\mathbf{x}) = \alpha(x^4+y^4) + \beta(x^2+y^2), \quad \alpha > 0,\ \beta < 0,\ \text{quadruple-well}. \tag{1.3}$$

* Corresponding author. Tel.: +886 4 22860133x619; fax: +886 4 22873028.
E-mail address: cschien@amath.nchu.edu.tw (C.-S. Chien).

0377-0427/$ – see front matter © 2010 Elsevier B.V. All rights reserved.
doi:10.1016/j.cam.2010.11.024

The sine function in (1.1) can be replaced by the cosine function. When $a = b = 0$ in (1.1), the GPE models BEC of weakly interacting atomic/molecular gases. When $a, b \neq 0$, the GPE models BEC in optical lattices [7–9].

Substituting the formula

$$\Psi(\mathbf{x}, t) = \mathrm{e}^{-\mathbf{i}\lambda t} u(\mathbf{x})$$

into (1.1), we obtain the stationary-state nonlinear eigenvalue problem

$$\begin{aligned} &F(u, \lambda) = -\Delta u - \lambda u + \left[V(\mathbf{x}) + a \sin^2\left(\frac{\pi x}{d}\right) + b \sin^2\left(\frac{\pi y}{d}\right)\right] u + \mu |u|^2 u = 0 \quad \text{in } \Omega, \\ &u = 0 \quad \text{on } \partial\Omega, \end{aligned} \tag{1.4}$$

respectively, where λ is the chemical potential which is proportional to the total energy of the system, and $u(\mathbf{x})$ the real wave function independent of t. It is well-known that the ground state as well as excited-states of (1.4) possess certain symmetry properties. In particular, these solutions can be obtained using the information of eigenstates of the corresponding linear Schrödinger eigenvalue problem (SEP). States of (1.4) obtained by this procedure are called states with linear counterparts. Vortices and solitons obtained in experiments are examples of excited-states with linear counterparts. However, the GPE may also admit states without linear counterparts. It is indicated in [10] that the generation of stationary states without linear counterparts can be understood in terms of bifurcations. In fact, it is more appropriate to interpret states without linear counterparts from the viewpoint of secondary bifurcations in semilinear elliptic eigenvalue problems. More precisely, states with linear counterparts correspond to primary bifurcations of the GPE, while states without linear counterparts correspond to secondary bifurcations.

During the past years, various numerical methods have been proposed to study quantum behavior of (1.1). For instance, Bao et al. [11–13] used the time-splitting spectral method to study the time-dependent GPE, where the Fourier spectral method was used to discretize the Laplacian, and the left hand side of (1.1) was integrated exactly. García-Ripoll and Pérez-García [14] exploited a version of the continuous steepest gradient, namely, the imaginary time evolution method (ITEM) to minimize the energy functional of (1.1) by using the Sobolev gradient of the energy functional as the preconditioner. Moreover, Crasovan et al. [15,16] studied the Newton type methods for vortex dipoles and parallel vortex rings in BEC. Bao and Du [17] presented a continuous normalized gradient flow (CNGF) to compute the ground-state solution of the BEC. Recently, Yang and Lakoba [18] proposed accelerated imaginary-time evolution methods (AITEMs) for computing solitary waves in arbitrary spatial dimensions, which have significantly improved the convergence rate of the ITEM. Muruganandam and Adhikari [19] studied pseudospectral and finite difference methods for the numerical solution of the BEC in three dimensions. Wang [20] used the split-step finite difference method for the numerical solution of (1.1). To the best of our knowledge, the second kind Chebyshev polynomials has never been implemented to solve the GPE.

To start with, we consider an operator equation of the following form

$$\begin{aligned} &F(u, \lambda) = -\Delta u + f(u, \lambda) = 0 \quad \text{in } \Omega = (0, 1)^2, \\ &u = 0 \quad \text{on } \partial\Omega, \end{aligned} \tag{1.5}$$

where $f : \mathbf{R} \to \mathbf{R}$ is a smooth odd function which satisfy

$$f(0, \lambda) = 0, \qquad f'(0, \lambda) \neq 0, \qquad f'''(0, \lambda) \neq 0. \tag{1.6}$$

It is clear that (1.4) is of the form (1.5) which satisfies (1.6). Due to $f(0, \lambda) = 0$, the operator Eq. (1.5) has a trivial solution curve $\{(0, \lambda) | \lambda \in \mathbf{R}\}$. A bifurcation point on the trivial solution curve of (1.5) is called a primary bifurcation point. A solution branch of (1.5) which bifurcates at a primary bifurcation point is called a primary solution curve. A bifurcation point on the primary solution curve is called a secondary bifurcation. A solution curve branching from a secondary bifurcation is called a secondary solution branch.

It is well-known that primary bifurcations of (1.4) possess certain symmetry properties. But the symmetries will no longer exist for secondary bifurcations. We refer to this phenomenon as symmetry-breaking bifurcation. In [21] the existence and stability of states of the GPE with linear counterparts has been studied in the discrete case. States without linear counterparts for the 1D BEC with double well potential were shown in [10]. Recently, a numerical continuation method was briefly described for the 1D GPE with double well potential in (1.3) where $\alpha > 0$, $\beta < 0$ [22]. To the best of our knowledge, modes of the 2D GPE without linear counterparts have rarely been investigated numerically. In this paper, we will study numerical continuation methods for symmetry-breaking solutions of (1.4). Recently, some numerical continuation algorithms have been developed for computing the ground state as well as the first few excited-state solutions of the NLS [23–25]. To find symmetry-breaking solutions of (1.4) using a numerical continuation algorithm, we first trace a primary solution curve, say, branching from the first excited-state bifurcation on the trivial solution curve. We detect singularity of the Fréchet derivative $D_u F$ along the primary solution curve. If a singularity is signalled, then we can switch from the primary solution to the secondary solution curve. We stop the curve-tracking whenever the mass conservation constraint

$$\int_\Omega |u|^2 \mathrm{d}\mathbf{x} \equiv N(u) \gg 1 \tag{1.7}$$

is satisfied. Note that we choose $N(u) \gg 1$ so that the nodal lines of symmetry-breaking solutions would be manifest. The constraint $N(u) = 1$ is widely used since other values may be scaled into the nonlinear coefficient μ [23–26].

This paper is organized as follows. In Section 2 we briefly review some basic theory for semilinear elliptic eigenvalue problems. We also discuss how to obtain symmetry-breaking solutions of the GPE via the states with linear counterparts. In Section 3 we derive a two-grid continuation discretization scheme for computing symmetry-breaking solutions of the GPE. In Section 4 we study spectral-Galerkin methods for SEP and GPE, where the second kind Chebyshev polynomials are used as the basis functions. Some basic formulae for the coefficient matrices of the discrete SEP are derived. Thus the eigenpairs of the discrete SEP can be easily evaluated. In Section 5 both the two-grid centered difference scheme and spectral-Galerkin method are used to discretize the GPE. Our numerical results show that symmetry-breaking solutions exist for various types of the GPE mentioned above. Finally, some concluding remarks are given in Section 6.

2. Basic theory for states with/without linear counterparts

In this section we will briefly review some basic theory for the semilinear elliptic eigenvalue problems (1.5). Next, we will show how numerical continuation methods can used to compute symmetry-breaking solutions of the GPE.

In the eighties of last century, bifurcations of semilinear elliptic eigenvalue problems have been extensively studied [27–29]. Numerical path-following techniques for symmetry-breaking solution curves of the fourth order von Kármán equations at multiple bifurcations (or degenerate energy levels in physics literatures) can be found in [30].

A function u is said to be Hölder continuous of exponent $s \in (0, 1)$ in $\bar{\Omega}$, the closure of Ω, if for any $(x, y),\ (x', y') \in \bar{\Omega}$, $|u(x, y) - u(x', y')| \le L\|(x, y) - (x', y')\|^s$ for some constant L. Let $C^{k,s}(\Omega)$ be the space of k-times differentiable functions u on $\bar{\Omega}$ such that u and its derivatives are Hölder continuous of exponent s. We define two spaces

$$X := \{u \in C^{2,s}(\Omega) \mid u|_{\partial\Omega} = 0\}, \qquad Y := C^{0,s}(\Omega) \tag{2.1}$$

endowed with the Hölder norms $\|\cdot\|_{2,s}$ and $\|\cdot\|_{0,s}$, respectively. Denote F_0 and D_uF_0 as the evaluations of F and D_uF at the bifurcation point $(u, \lambda) = (0, \lambda_0)$. It is well-known in elliptic partial differential equation that the derivative

$$D_uF_0 = -\Delta + \lambda_0 Id : X \to Y \tag{2.2}$$

is self-adjoint and a Fredholm operator of index zero [31]. Then $R(D_uF_0) = N(D_uF_0)^{\perp}$ and

$$X = N(D_uF_0) \oplus N(D_uF_0)^{\perp}, \tag{2.3}$$

where $N(G)$ and $R(G)$ denote the null space and range of an operator G, respectively, and $\oplus$ represents the direct sum under the inner product in $L^2(\Omega)$. Since $D_\lambda F_0 = 0$, we have $R(DF_0) = R(D_uF_0) = N(D_uF_0)^{\perp}$. Thus if $m = \dim N(D_uF_0)$, then $(0, \lambda_0)$ is called a corank-m or m-fold degenerate bifurcation point of (1.5).

We are concerned with two-fold degenerate bifurcation points [32] of the form $(0, \lambda_0) = (0, (m^2 + n^2)\pi^2),\ m \ne n$, where

$$N(D_uF_0) = \operatorname{span}\{\phi_1, \phi_2\} \text{ with } \begin{array}{l} \phi_1 := 2\sin m\pi x \cdot \sin n\pi y, \\ \phi_2 := 2\sin n\pi x \cdot \sin m\pi y. \end{array} \tag{2.4}$$

Solution branches of (1.5) with nodal lines parallel to the x-and y-axis in a neighborhood of $(0, \lambda_0)$ are called rectangular solution branches. Rectangular solution branches have the same nodal line structure as the eigenfunctions of the Laplacian. Note that we also have

$$N(D_uF_0) = \operatorname{span}\{\phi_1 + \phi_2, \phi_1 - \phi_2\}. \tag{2.5}$$

Solution branches of (1.5) which have the same local nodal line structures as the basis in (2.5) are called triangular solution branches [28]. Using a modified Lyapunov–Schmidt method it has been shown in [27] that (1.5) has exactly four nontrivial different solution branches passing through a two-fold degenerate bifurcation point, namely, two rectangular solution curves and two triangular solution curves.

To compute an energy level of (1.4) using continuation algorithms, we can trace the corresponding solution curve branching from a bifurcation point on the trivial solution curve $\{(0, \lambda) | \lambda \in \mathbf{R}\}$. We stop the curve-tracking whenever the mass conservation constraint (1.7) is satisfied for some chemical value $\tilde{\lambda}$. We denote $(\tilde{u}, \tilde{\lambda})$ as a target point in the curve-tracking. Note that the parameter of a bifurcation $(0, \lambda^*)$ on the trivial solution curve of the GPE is just an eigenvalue of the associated SEP. We can detect bifurcation points along the trivial solution curve of (1.4) by monitoring the singularity of the Fréchet derivative D_uF. However, the computational cost can be very expensive if the order of D_uF is large. In practice, we may compute the first few eigenpairs of (1.5) using some well-known software packages. Thus continuation methods can compute states of the GPE with linear counterparts.

Next, we will detect secondary bifurcation points along the primary rectangular solution branch/triangular solution branch bifurcating at $(0, \lambda_{1,2}) = (0, 5\pi^2)$. Thus we need to monitor the singularity of D_uF using some numerical methods. If a bifurcation point is detected on the primary solution branch, then we may switch from the primary solution curve to the secondary solution curve using a local perturbation or some branch-switching techniques. We trace the secondary solution branch until the constraint (1.7) is satisfied. The procedure shows that continuation methods can compute states of (1.4) without linear counterparts via states with linear counterparts.

3. Computing secondary bifurcations on the fine grid

In this section, we will describe two efficient numerical methods for detecting secondary bifurcations of the 2D GPE on the fine grid in the context of a two-grid centered difference discretization scheme. In particular, we will use the information of a secondary bifurcation obtained on the coarse grid to compute its counterpart on the fine grid. Let $\tilde{h}$, $h \in (0, 1)$ be properly chosen with $h < \tilde{h}$.

(I) Let $\tilde{c}$ and c be the associated primary solution curves of (1.5) on the coarse grid and fine grid, respectively. Let $(u_{\tilde{h}}^{(i)}, \lambda_{\tilde{h}}^{(i)})$ be a secondary bifurcation on $\tilde{c}$. Intuitively, to compute the associated secondary bifurcation on the fine grid, we can interpolate the state variable $u_{\tilde{h}}^{(i)}$ from the coarse space to the fine space. More precisely, let $\pi_{\tilde{h}}^{h} : \mathbf{R}^{\widetilde{N}^2 \times \widetilde{N}^2} \to \mathbf{R}^{N^2 \times N^2}$ be the interpolation operator such that $\pi_{\tilde{h}}^{h}(u_{\tilde{h}}^{(i)}) = \hat{u}_h \in \mathbf{R}^{N^2 \times N^2}$, where $\tilde{h} = 1/(\widetilde{N}+1)$ and $h = 1/(N+1)$ for some positive integers $\widetilde{N} < N$. Then we use $(\hat{u}_h, \lambda_{\tilde{h}}^{(i)})$ as an initial guess for the Newton iteration. Let $(u_h^{(i)}, \lambda_h^{(i)})$ be an approximating point on the solution curve c. If $(\hat{u}_h, \lambda_{\tilde{h}}^{(i)})$ is close enough to some neighborhood of $(u_h^{(i)}, \lambda_h^{(i)})$, then in general, only a few Newton iterations are required so that $(\hat{u}_h, \lambda_{\tilde{h}}^{(i)})$ will converge to $(u_h^{(i)}, \lambda_h^{(i)})$.

Next, we start with $(u_h^{(i)}, \lambda_h^{(i)})$, and use the predictor–corrector continuation method to trace the solution curve c on the fine grid. Meanwhile, we also detect secondary bifurcations along the solution curve c. If a secondary bifurcation point $(u_h^{(j)}, \lambda_h^{(j)}), j > i$, is detected on c, then we can use a local perturbation technique to switch from the primary solution branch to the secondary solution branch. More precisely, instead of solving (1.5), we solve

$$F(u, \lambda) + d = 0 \tag{3.1}$$

for branch-switching, where $d \in \mathbf{R}^{N^2}$ is a perturbation vector yet to be determined. In general, we choose d as the eigenvector of the discrete SEP. We stop the curve-tracking whenever the target point on the secondary solution curve is reached. That is, the constraint condition (1.7) is satisfied.

(II) A more delicate numerical method is to apply the two-grid discretization scheme [33] to compute the secondary bifurcation point on the fine grid. Let $(u_{\tilde{h}}, \lambda_{\tilde{h}}) \in \mathbf{R}^{\widetilde{N}^2} \times \mathbf{R}$ be a secondary bifurcation point on $\tilde{c}$. The centered difference analogue of (1.5) on the coarse grid is

$$A_{\tilde{h}} u_{\tilde{h}} + f(u_{\tilde{h}}, \lambda_{\tilde{h}}) = 0, \tag{3.2}$$

where $A_{\tilde{h}} \in \mathbf{R}^{\widetilde{N}^2 \times \widetilde{N}^2}$ is the coefficient matrix corresponding to the Laplacian $-\Delta$, and $f(u_{\tilde{h}}, \lambda_{\tilde{h}}) = [f((u_{\tilde{h}})_1, \lambda_{\tilde{h}}), f((u_{\tilde{h}})_2, \lambda_{\tilde{h}}), \ldots, f((u_{\tilde{h}})_{\widetilde{N}^2}, \lambda_{\tilde{h}})]^T \in R^{\widetilde{N}^2}$. Let $(u, \lambda_{\tilde{h}})$ be an exact solution of (1.5). We fix the parameter $\lambda_{\tilde{h}}$ so that we can make a correction for the state variable $u_{\tilde{h}}$ on the fine grid. The linear approximation of the mapping $F(u, \lambda_{\tilde{h}})$ at $u_{\tilde{h}}$ is

$$0 = F(u, \lambda_{\tilde{h}}) \approx F(u_{\tilde{h}}, \lambda_{\tilde{h}}) + D_u F(u_{\tilde{h}}, \lambda_{\tilde{h}})(u - u_{\tilde{h}}). \tag{3.3}$$

Setting $e = u - u_{\tilde{h}}$, Eq. (3.3) is equivalent to

$$D_u F(u_{\tilde{h}}, \lambda_{\tilde{h}}) e \approx -F(u_{\tilde{h}}, \lambda_{\tilde{h}}), \tag{3.4}$$

where the Fréchet derivative $D_u F(u_{\tilde{h}}, \lambda_{\tilde{h}}) = -\Delta + D_u f(u_{\tilde{h}}, \lambda_{\tilde{h}})$. It follows from (1.5) and (3.4) that the approximate solution $u_{\tilde{h}}$ on the coarse grid can be corrected by solving

$$\begin{aligned} &-\Delta e + D_u f(u_{\tilde{h}}, \lambda_{\tilde{h}}) e = \Delta u_{\tilde{h}} - f(u_{\tilde{h}}, \lambda_{\tilde{h}}) \quad \text{in } \Omega, \\ &e = 0 \quad \text{on } \partial\Omega \end{aligned} \tag{3.5}$$

on the fine grid. The centered difference analogue of (3.5) is

$$(A_h + B_h(u_h, \lambda_{\tilde{h}})) e_h = -A_h(I_{\tilde{h}}^h u_{\tilde{h}}) - f(I_{\tilde{h}}^h u_{\tilde{h}}, \lambda_{\tilde{h}}), \tag{3.6}$$

where A_h is the coefficient matrix corresponding to $-\Delta$ on the fine grid, e_h the solution of (3.5) yet to be determined, and

$$B_h(u_h, \lambda_{\tilde{h}}) = \operatorname{diag}\left(D_u f((I_{\tilde{h}}^h u_{\tilde{h}})_1, \lambda_{\tilde{h}}), D_u f((I_{\tilde{h}}^h u_{\tilde{h}})_2, \lambda_{\tilde{h}}), \ldots, D_u f((I_{\tilde{h}}^h u_{\tilde{h}})_{N^2}, \lambda_{\tilde{h}})\right) \in \mathbf{R}^{N^2 \times N^2},$$

$$f(I_{\tilde{h}}^h u_{\tilde{h}}, \lambda_{\tilde{h}}) = \left[f((I_{\tilde{h}}^h u_{\tilde{h}})_1, \lambda_{\tilde{h}}), f((I_{\tilde{h}}^h u_{\tilde{h}})_2, \lambda_{\tilde{h}}), \ldots, f((I_{\tilde{h}}^h u_{\tilde{h}})_{N^2}, \lambda_{\tilde{h}})\right]^T \in \mathbf{R}^{N^2}.$$

In order to obtain an accurate parameter λ_h on the fine grid, we set

$$\hat{u}_h = I_{\tilde{h}}^h u_{\tilde{h}} + e_h$$

and compute the Rayleigh quotient

$$\hat{\lambda}_h = -\frac{(\hat{u}_h)^T A_h \hat{u}_h}{(\hat{u}_h)^T f(\hat{u}_h, \lambda_{\tilde{h}})},$$

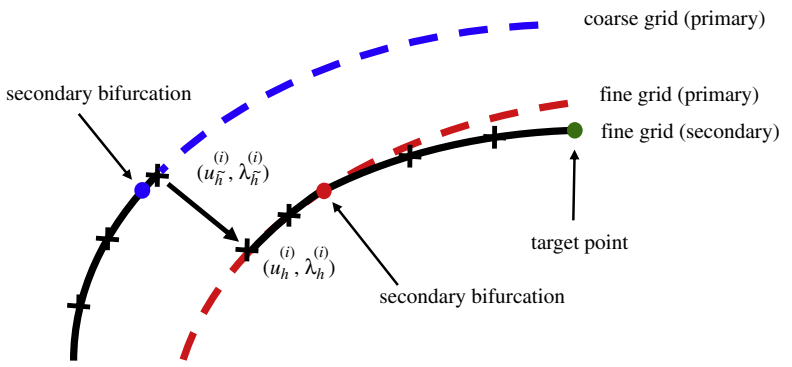

Fig. 1. The diagram of the two-grid continuation algorithm for symmetry-breaking solutions of the GPE.

where $f(\hat{u}_h, \lambda_{\tilde{h}}) = \left[f((\hat{u}_h)_1, \lambda_{\tilde{h}}), f((\hat{u}_h)_2, \lambda_{\tilde{h}}), \ldots, f((\hat{u}_h)_{N^2}, \lambda_{\tilde{h}})\right]^T \in \mathbf{R}^{N^2}$. Now use $(\hat{u}_h, \hat{\lambda}_h)$ as an initial guess, and perform Newton's method until the iteration converges to an approximating point $(u_h^{(i)}, \lambda_h^{(i)})$ on the solution curve c. Next, we use $(u_h^{(i)}, \lambda_h^{(i)})$ as a starting point and use the predictor–corrector continuation algorithm to trace the solution curve c. We also detect secondary bifurcations along the solution curve. The remaining procedures are the same as those of (I), and will not be stated here. The two-grid continuation algorithm for computing symmetry-breaking solution of the GPE is given as follows.

Algorithm 3.1. A two-grid continuation algorithm for computing symmetry-breaking solutions of the GPE.

Input:

$\varepsilon :=$ accuracy tolerance for the Newton corrector on each level of grids.

$\tilde{h} :=$ coarse grid size.

$h :=$ fine grid size.

$(u_{\tilde{h}}^{(0)}, \lambda_{\tilde{h}}^{(0)}) :=$ starting approximating point for the solution curve $\tilde{c}$ on the coarse grid.

1. Compute the desired eigenpair of the linearized problem on the coarse grid.
2. Outer continuation.
   Use a predictor–corrector continuation algorithm to trace the solution curve on the coarse grid until the secondary bifurcation point $(u_{\tilde{h}}^{(i)}, \lambda_{\tilde{h}}^{(i)})$ is detected.
3. Inner continuation.
   (i) Predictor.
   Set $(I_{\tilde{h}}^h u_{\tilde{h}}^{(i)}, \lambda_{\tilde{h}}^{(i)})$ as the predicted point.
   (ii) Corrector.
   (a) Make a correction on the fine grid: solve the linear system
   $$(A_h + B_h(u_h^{(i)}, \lambda_{\tilde{h}}^{(i)}))e_h = -A_h(I_{\tilde{h}}^h u_{\tilde{h}}^{(i)}) - f(I_{\tilde{h}}^h u_{\tilde{h}}^{(i)}, \lambda_{\tilde{h}}^{(i)}).$$
   (b) Set $\hat{u}_h = I_{\tilde{h}}^h u_{\tilde{h}}^{(i)} + e_h$.
   (c) Compute $\hat{\lambda}_h = -\frac{(\hat{u}_h)^T A_h \hat{u}_h}{(\hat{u}_h)^T f(\hat{u}_h, \lambda_{\tilde{h}})}$.
   (d) If $\|F(\hat{u}_h, \hat{\lambda}_h)\| < \varepsilon$, then
   accept $(\hat{u}_h, \hat{\lambda}_h)$ as an approximating point on the fine grid,
   set $u_h^{(i)} = \hat{u}_h, \lambda_h^{(i)} = \hat{\lambda}_h$.
   Else if $\|F(\hat{u}_h, \hat{\lambda}_h)\| > \varepsilon$, then
   use $(\hat{u}_h, \hat{\lambda}_h)$ as an initial guess and perform Newton's method until the iterates converges to $(u_h^{(i)}, \lambda_h^{(i)})$, an approximating point on the fine grid.
   End if.
4. Use $(u_h^{(i)}, \lambda_h^{(i)})$ as a starting point and use a predictor–corrector continuation algorithm to trace the primary solution curve on the fine grid. Meanwhile, detect secondary bifurcations along the solution curve.
5. If a secondary bifurcation point $(u_h^{(j)}, \lambda_h^{(j)}), j > i$, is detected, then use the local perturbation technique to switch from the primary solution branch to the secondary solution branch, and trace the secondary solution curve until the target point is reached.
   End if.

The solid line in Fig. 1 displays the solution curve of (1.5) we wish to trace in Algorithm 3.1, and the dashed line represents the solution curve we do not have to trace.

4. Chebyshev-spectral-Galerkin methods

The second kind Chebyshev polynomials are defined by the following recursive formula [4]

$$U_k(x) = \sin(k+1)\theta/\sin\theta \quad \text{when } x = \cos\theta,\ \theta \in [0,\pi] \Leftrightarrow x \in [-1,1]. \tag{4.1}$$

Note that $U_k(x)$ is a polynomial of degree k. The first few terms are

$$U_0(x) = 1, \qquad U_1(x) = 2x, \qquad U_2(x) = 4x^2 - 1, \ldots, \quad k = 0, 1, 2, \ldots.$$

The set of polynomials $\{U_k(x)\}_{k=0}^{\infty}$ forms an orthogonal system on the Hilbert space $L_w^2[-1,1]$ with respect to the inner product $(\cdot,\cdot)_w$ defined by $(f,g)_w = \int_{-1}^{1} fgw\,dx$, where $w(x) = (1-x^2)^{1/2}$. We have

$$(U_i(x), U_j(x))_w = \frac{\pi}{2}\delta_{ij}, \quad \forall i, j \geq 0. \tag{4.2}$$

In this section, we will study spectral-Galerkin method using the second kind Chebyshev polynomials for the numerical solutions of the GPE. First we consider the SEP

$$\begin{aligned} &F(u,\lambda) = -\Delta u(x) + V(x)u(x) - \lambda u(x) = 0 \quad \text{in } \Omega = (-1,1)^d,\ d = 1, 2,\\ &u = 0 \quad \text{on } \partial\Omega. \end{aligned} \tag{4.3}$$

4.1. 1D SEP

Let S_N^1 be the subspace spanned by $\{U_0(x), U_1(x), \ldots, U_N(x)\}$. We choose the trial function space V_N^1 as

$$V_N^1 = \{v \in S_N^1 : v(\pm 1) = 0\}.$$

Since $U_k(\pm 1) = (\pm 1)^k(k+1)$, it is clear that the functions $U_k(x)$ do not satisfy the boundary conditions of the GPE. Thus we construct a set of basis functions $\{\phi_k(x)\}$ for V_N^1 by setting

$$\phi_k(x) = \frac{U_k(x)}{k+1} - \frac{U_{k+2}(x)}{k+3}, \quad k = 0, 1, \ldots, N-2. \tag{4.4}$$

We have

$$\phi_0(x) = -\frac{4}{3}x^2 + \frac{4}{3}, \qquad \phi_1(x) = -2x^3 + 2x, \qquad \phi_2(x) = -\frac{16}{5}x^4 + \frac{56}{15}x^2 - \frac{8}{15}, \ldots.$$

It follows that $\phi_k(x) \in V_N^1$ and $\{\phi_k(x)\}_{k=0}^{N-2}$ are linearly independent. Thus $V_N^1 = \operatorname{span}\{\phi_0(x), \phi_1(x), \ldots, \phi_{N-2}(x)\}$ with $\dim V_N^1 = N-1$.

The Chebyshev–Galerkin formulation for (4.3) with $V(x) = 0$ in 1D is to find $u_N = \sum_{k=0}^{N-2} \alpha_k\phi_k(x) \in V_N^1$ such that

$$(-u_N'', v)_w = \lambda(u_N, v)_w, \quad \forall v \in V_N^1, \tag{4.5}$$

where α_k are the unknown coefficients yet to be determined.

Setting $v = \phi_k(x)$ in (4.5), $k = 0, 1, \ldots, N-2$, we obtain the associated matrix eigenvalue problem

$$A_1\alpha = \lambda B_1\alpha, \tag{4.6}$$

where $\alpha = (\alpha_0, \alpha_1, \ldots, \alpha_{N-2})^T$, $A_1 = (a_{kj})_{0\leq k,j\leq N-2}$, and $B_1 = (b_{kj})_{0\leq k,j\leq N-2}$ with

$$a_{kj} = -(\phi_j''(x), \phi_k(x))_w \quad \text{and} \quad b_{kj} = (\phi_j(x), \phi_k(x))_w. \tag{4.7}$$

The following lemma is the key to the efficiency of our algorithm.

Lemma 4.1. *Let $\phi_k(x)$ and a_{kj}, b_{kj} be defined as in (4.4) and (4.7), respectively. We have*

$$a_{kj} = \begin{cases} \dfrac{2k+4}{k+3}\pi, & j = k,\\ -2\pi(k+2)\left(\dfrac{1}{j+1} - \dfrac{1}{j+3}\right), & j = k+2, k+4, k+6, \ldots,\\ 0, & j < k \text{ or } j+k \text{ odd}, \end{cases} \tag{4.8}$$

and

$$b_{kj} = \begin{cases} \dfrac{\pi}{2}\left[\dfrac{1}{(k+1)^2} + \dfrac{1}{(k+3)^2}\right], & j = k,\\ -\dfrac{\pi}{2}\dfrac{1}{(k+3)^2}, & j = k+2,\\ -\dfrac{\pi}{2}\dfrac{1}{(k+1)^2}, & j = k-2,\\ 0, & \textit{otherwise}. \end{cases} \tag{4.9}$$

Proof. The proofs of (4.8) and (4.9) are based on the following well-known property of the second kind Chebyshev polynomials [4, (1.7) and (2.48)]

$$2(n+1)U_n = U'_{n+1} - U'_{n-1}. \tag{4.10}$$

By a simple computation using (4.10), we derive

$$\begin{aligned} U''_n(x) &= (2n)(2n-2)U_{n-2}(x) + [(2n)(2n-6) + (2n-4)(2n-6)]\,U_{n-4}(x) \\ &\quad + [(2n)(2n-10) + (2n-4)(2n-10) + (2n-8)(2n-10)]\,U_{n-6}(x) + \cdots \\ &= \sum_{\substack{k=0 \\ k+n \text{ even}}}^{n-2} \left\{ 4 \left[(k+1) \sum_{\substack{i=k+2 \\ i+n \text{ even}}}^{n} i \right] U_k(x) \right\}, \end{aligned} \tag{4.11}$$

and

$$\begin{aligned} U''_{n+2}(x) &= (2n+4)(2n+2)U_n(x) + [(2n+4)(2n-2) + (2n)(2n-2)]\,U_{n-2}(x) \\ &\quad + [(2n+4)(2n-6) + (2n)(2n-6) + (2n-4)(2n-6)]\,U_{n-4}(x) + \cdots. \end{aligned} \tag{4.12}$$

Using (4.2) we obtain

$$\begin{aligned} b_{kj} &= \left(\frac{U_j(x)}{j+1}, \frac{U_k(x)}{k+1} \right)_w - \left(\frac{U_j(x)}{j+1}, \frac{U_{k+2}(x)}{k+3} \right)_w - \left(\frac{U_{j+2}(x)}{j+3}, \frac{U_k(x)}{k+1} \right)_w + \left(\frac{U_{j+2}(x)}{j+3}, \frac{U_{k+2}(x)}{k+3} \right)_w \\ &= \begin{cases} \dfrac{\pi}{2} \left[\dfrac{1}{(k+1)^2} + \dfrac{1}{(k+3)^2} \right], & j = k, \\ -\dfrac{\pi}{2} \dfrac{1}{(k+3)^2}, & j = k+2, \\ -\dfrac{\pi}{2} \dfrac{1}{(k+1)^2}, & j = k-2, \\ 0, \ \text{otherwise}. \end{cases} \end{aligned}$$

Next, for $j < k$ or $j + k$ is odd, it follows immediately from (4.2) and (4.12) that

$$\begin{aligned} a_{kj} &= -(\phi''_j(x), \phi_k(x))_w \\ &= -\left(\frac{U''_j(x)}{j+1}, \frac{U_k(x)}{k+1} \right)_w + \left(\frac{U''_j(x)}{j+1}, \frac{U_{k+2}(x)}{k+3} \right)_w + \left(\frac{U''_{j+2}(x)}{j+3}, \frac{U_k(x)}{k+1} \right)_w - \left(\frac{U''_{j+2}(x)}{j+3}, \frac{U_{k+2}(x)}{k+3} \right)_w \\ &= 0, \end{aligned}$$

and

$$a_{kk} = -(\phi''_k(x), \phi_k(x))_w = \left(\frac{U''_{k+2}(x)}{k+3}, \frac{U_k(x)}{k+1} \right)_w = \frac{2k+4}{k+3}\pi.$$

Setting $-\phi''_j(x) = -\frac{U''_j(x)}{j+1} + \frac{U''_{j+2}(x)}{j+3} = \sum_{n=0}^{j} d_n U_n(x)$, we derive

$$d_{j-2i} = -\frac{1}{j+1}(2j-2i+2)(2j-4i+2)i + \frac{1}{j+3}(2j-2i+4)(2j-4i+2)(i+1), \quad \text{for } i = 1, 2, 3, \ldots.$$

Hence for $j = k + 2i$, $i = 1, 2, 3, \ldots$, we find

$$\begin{aligned} -(\phi''_j(x), \phi_k(x))_w &= \left(d_j U_j(x) + d_{j-2}U_{j-2}(x) + d_{j-4}U_{j-4}(x) + \cdots, \frac{U_k(x)}{k+1} - \frac{U_{k+2}(x)}{k+3} \right)_w \\ &= \left(d_k U_k(x), \frac{U_k(x)}{k+1} \right)_w - \left(d_{k+2}U_{k+2}(x), \frac{U_{k+2}(x)}{k+3} \right)_w \\ &= \frac{d_{j-2i}}{j-2i+1}(U_k(x), U_k(x))_w - \frac{d_{j-2i+2}}{j-2i+3}(U_{k+2}(x), U_{k+2}(x))_w \\ &= -2\pi(k+2)\left(\frac{1}{j+1} - \frac{1}{j+3} \right). \quad \square \end{aligned}$$

Similarly, when $V(x) = \frac{1}{2}x^2$, the spectral-Galerkin formulation for (4.3) is to find $u_N = \sum_{k=0}^{N-2} \alpha_k \phi_k(x) \in V_N^1$ such that

$$(-u_N'', v)_w + \frac{1}{2}(x^2 u_N, v)_w = \lambda(u_N, v)_w, \quad \forall v \in V_N^1.$$

The associated matrix eigenvalue problem is

$$\left(A_1 + \frac{1}{2}C\right)\alpha = \lambda B_1 \alpha, \tag{4.13}$$

where A_1 and B_1 are defined as in (4.13), and $C = (c_{kj})_{0\le k,j\le N-2}$ with

$$c_{kj} = (x^2\phi_j(x), \phi_k(x))_w. \tag{4.14}$$

The following lemma is also the key to the efficiency of our algorithms.

Lemma 4.2. *Let $\phi_k(x)$ and c_{kj} be defined as in (4.4) and (4.14). Then*

$$c_{kj} = \begin{cases} \dfrac{\pi}{4}\left[\dfrac{r_j}{(j+1)^2} + \dfrac{1}{(j+3)^2} - \dfrac{1}{(j+1)(j+3)}\right], & j = k, \\ \dfrac{\pi}{(s+1)(s+3)^2(s+5)}, & |j-k| = 2, \\ \dfrac{\pi}{8(s+3)(s+5)}, & |j-k| = 4, \\ 0, \quad \textit{otherwise}, \end{cases}$$

where $r_0 = \dfrac{1}{2}$, $r_i = 1$ *for* $i \ge 1$, *and* $s = \min\{j, k\}$.

Proof. Note that

$$\begin{aligned} c_{kj} = {} & \frac{1}{(j+1)(k+1)}\left(x^2U_j(x), U_k(x)\right)_w - \frac{1}{(j+1)(k+3)}\left(x^2U_j(x), U_{k+2}(x)\right)_w \\ & - \frac{1}{(j+3)(k+1)}\left(x^2U_{j+2}(x), U_k(x)\right)_w + \frac{1}{(j+3)(k+3)}\left(x^2U_{j+2}(x), U_{k+2}(x)\right)_w. \end{aligned}$$

By a simple computation, we derive

$$\begin{aligned} \left(x^2U_j(x), U_k(x)\right)_w = {} & \frac{1}{4}\int_0^\pi \cos(j-k)\theta - \cos(j+k+2)\theta + \frac{1}{2}[\cos(2+j-k)\theta \\ & + \cos(2-j+k)\theta - \cos(4+j+k)\theta - \cos(-j-k)\theta]\,\mathrm{d}\theta. \end{aligned}$$

Thus, we have

$$(x^2U_j(x), U_k(x))_w = \begin{cases} \dfrac{\pi}{8}, & j = k = 0, \\ \dfrac{\pi}{4}, & j = k \ne 0, \\ \dfrac{\pi}{8}, & |j-k| = 2, \\ 0, \quad \text{otherwise}, \end{cases} \qquad (x^2U_j(x), U_{k+2}(x))_w = \begin{cases} \dfrac{\pi}{8}, & j = k, \\ \dfrac{\pi}{4}, & j-k = 2, \\ \dfrac{\pi}{8}, & j-k = 4, \\ 0, \quad \text{otherwise}, \end{cases}$$

$$(x^2U_{j+2}(x), U_k(x))_w = \begin{cases} \dfrac{\pi}{8}, & j = k, \\ \dfrac{\pi}{4}, & k-j = 2, \\ \dfrac{\pi}{8}, & k-j = 4, \\ 0, \quad \text{otherwise}, \end{cases} \quad \text{and} \quad (x^2U_{j+2}(x), U_{k+2}(x))_w = \begin{cases} \dfrac{\pi}{4}, & j = k, \\ \dfrac{\pi}{8}, & |j-k| = 2, \\ 0, \quad \text{otherwise}. \end{cases}$$

Therefore, if $j = k$, we have

$$c_{kk} = \begin{cases} \dfrac{5\pi}{72}, & k = 0, \\ \dfrac{\pi}{4}\left[\dfrac{1}{(j+1)^2} + \dfrac{1}{(j+3)^2} - \dfrac{1}{(j+1)(j+3)}\right], & k \ne 0. \end{cases}$$

For $j \neq k$, we have

$$c_{kj} = \begin{cases} \dfrac{\pi}{(s+1)(s+3)^2(s+5)}, & |j-k| = 2, \\ \dfrac{\pi}{8(s+3)(s+5)}, & |j-k| = 4, \\ 0, \quad \text{otherwise.} \end{cases} \qquad \text{where } s = \min\{j,k\}. \quad \square$$

4.2. 2D SEP

Let $V_N^2 = \text{span}\{\phi_k(x)\phi_j(y) : k,j = 0,1,\ldots,N-2\}$ where $\phi_k(x)$ and $\phi_j(y)$ are defined as in the 1D case. The Chebyshev–Galerkin approximation for (4.3) with $V(\mathbf{x}) = 0$ in 2D is to find $u_N = \sum_{k,j=0}^{N-2} \alpha_{kj}\phi_k(x)\phi_j(y)$ such that

$$(-\Delta u_N, v)_w = \lambda(u_N, v)_w \quad \forall v \in V_N^2, \tag{4.15}$$

where $w(x,y) = \sqrt{1-x^2}\sqrt{1-y^2}$ is the weight function of second kind Chebyshev polynomials. Taking $v = \phi_l(x)\phi_m(y)$ in (4.15) for $l, m = 0, 1, \ldots, N-2$, we obtain the following matrix equation:

$$A_1 U B_1 + B_1 U A_1^T = \lambda B_1 U B_1, \tag{4.16}$$

where A_1 and B_1 are the matrices defined in (4.6) and $U = (\alpha_{kj})_{0\le k,j\le N-2}$ is the unknown coefficients matrix. Eq. (4.16) can be simplified by the following proposition [34, Proposition 7.1.9].

Proposition 4.3. *Let $A \in \mathbf{F}^{n\times m}$, $B \in \mathbf{F}^{m\times l}$, and $C \in \mathbf{F}^{l\times k}$. Then*

$$\text{vec}(ABC) = (C^T \otimes A)\text{vec}\, B,$$

where vec *A is defined as the column vector of size $nm \times 1$ obtained by stacking the columns of A, and $\otimes$ is the Kronecker product.*

Applying Proposition 4.3 to (4.16), we obtain

$$(B_1^T \otimes A_1 + A_1 \otimes B_1)\text{vec}\, U = \lambda(B_1^T \otimes B_1)\text{vec}\, U,$$

which is a matrix eigenvalue problem. Similarly, when $V(\mathbf{x}) = \frac{1}{2}(x^2+y^2)$ we can derive from (4.3) the following matrix eigenvalue problem

$$\left(B_1^T \otimes A_1 + A_1 \otimes B_1 + \frac{1}{2}B_1^T \otimes C^x + \frac{1}{2}C^y \otimes B_1\right)\text{vec}\, U = \lambda(B_1^T \otimes B_1)\text{vec}\, U,$$

where

$$C^x = (x^2\phi_j(x), \phi_k(x))_w \quad \text{and} \quad C^y = (y^2\phi_j(y), \phi_k(y))_w, \quad 0 \le k, j \le N-2.$$

4.3. 2D GPE in a periodic potential

Next, we consider the 2D GPE in a periodic potential

$$\begin{aligned} &F(u,\lambda) = -\Delta u(\mathbf{x}) + [V(\mathbf{x}) + P(\mathbf{x}) - \lambda]u(\mathbf{x}) + \mu|u(\mathbf{x})|^2 u(\mathbf{x}) = 0 \quad \text{in } \Omega = (-1,1)^2, \\ &u = 0 \quad \text{on } \partial\Omega, \end{aligned} \tag{4.17}$$

where $V(\mathbf{x}) = \frac{1}{2}(x^2+y^2)$ and the periodic potential $P(\mathbf{x}) = a\sin^2\left(\frac{\pi x}{d}\right) + b\sin^2\left(\frac{\pi y}{d}\right)$. The weak formulation for (4.17) is to find $u_N \in V_N^2$ such that

$$(-\Delta u_N, v)_w + (V(\mathbf{x})u_N, v)_w + (P(\mathbf{x})u_N, v)_w + \mu(|u_N|^2 u_N, v)_w = \lambda(u_N, v)_w \quad \forall v \in V_N^2. \tag{4.18}$$

We can use Lemmas 4.1 and 4.2 to evaluate the values of $(-\Delta u_N, v)_w$, $(u_N, v)_w$, and $(V(\mathbf{x})u_N, v)_w$. The integrals $(P(\mathbf{x})u_N, v)_w$ and $\mu(|u_N|^2 u_N, v)_w$ can be evaluated using the following Gauss–Chebyshev quadrature formula (see [4, Theorem 8.4]).

Lemma 4.4. *The Gauss–Chebyshev formula is given by*

$$\int_{-1}^{1}\int_{-1}^{1} f(x,y)w(x,y)\,dx\,dy \simeq \sum_{i=1}^{n}\sum_{j=1}^{n} A_i A_j f(x_i) f(y_j),$$

where $\{x_i\}$ and $\{y_j\}$ are the n zeros of $\phi_n(x)$ and $\phi_n(y)$, respectively, and the coefficients $A_i = \frac{\pi}{n+1}(1-x_i^2)$, and $A_j = \frac{\pi}{n+1}(1-y_j^2)$.

Now it is straight forward to incorporate the Chebyshev-spectral-Galerkin methods in the context of a predictor–corrector continuation algorithm for computing the numerical solutions of the GPE.

5. Numerical results

The numerical methods described in the previous sections were exploited to investigate symmetry-breaking solutions of the GPE with parabolic and quadruple-well potentials. The value λ^* shown in the caption denotes the energy level of the

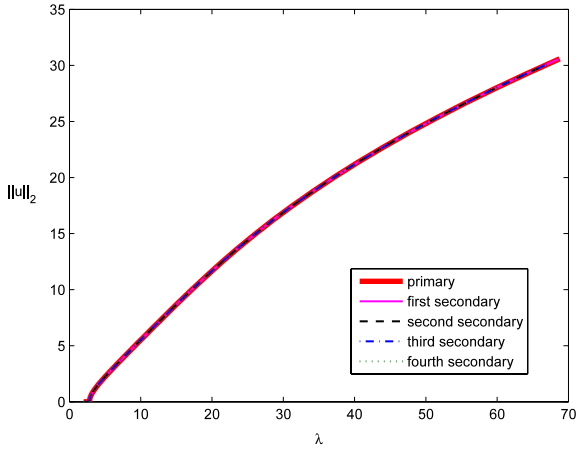

(a) Solution curves.

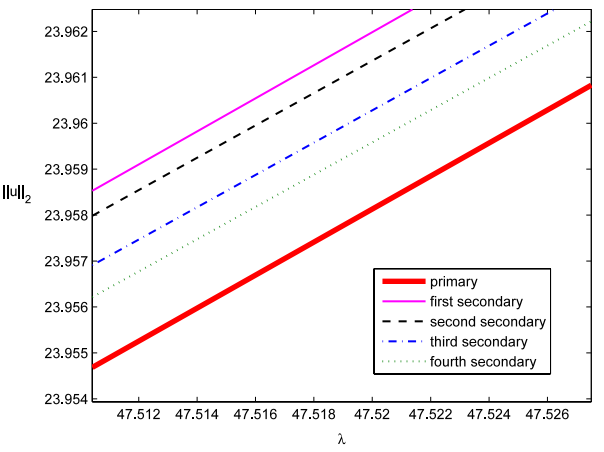

(b) Partial enlarged figure of (a).

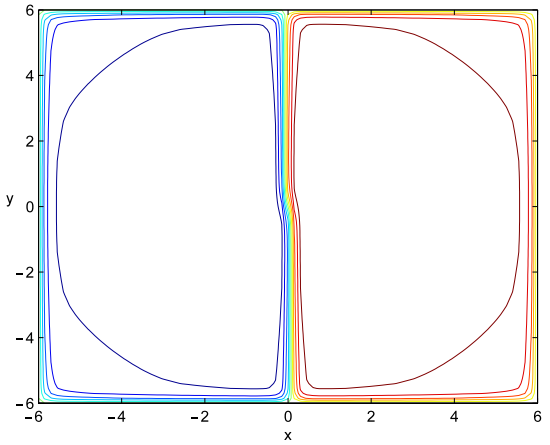

(c) The first secondary solution branch, where $\lambda^* \approx 30.8688$.

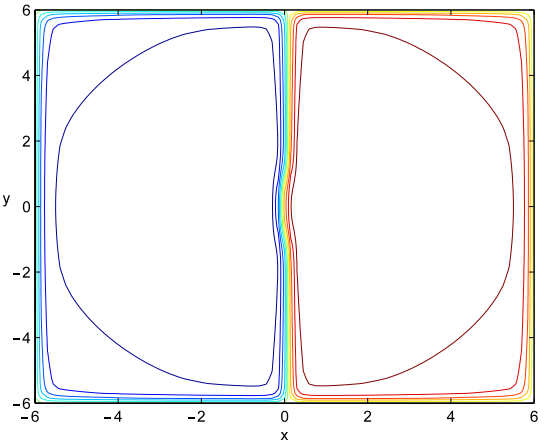

(d) The second secondary solution branch, where $\lambda^* \approx 38.9309$.

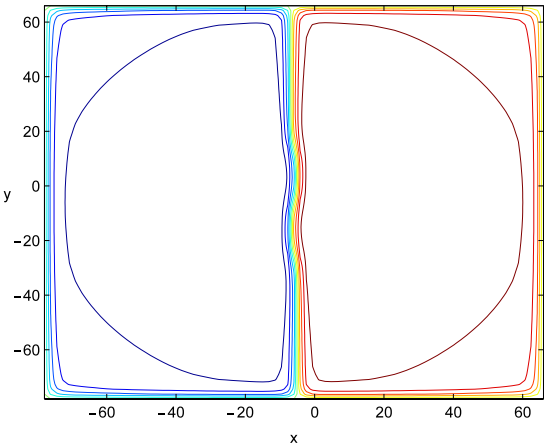

(e) The third secondary solution branch, where $\lambda^* \approx 44.0069$.

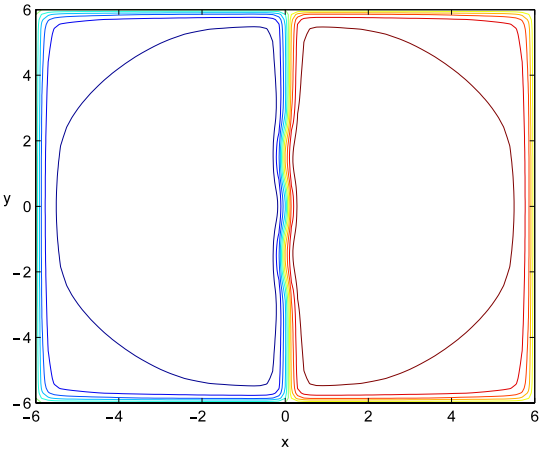

(f) The fourth secondary solution branch, where $\lambda^* \approx 48.2702$.

Fig. 2. The primary and first four secondary solution curves, and contours of the secondary solution curves associated with the first excited-state solution of (5.1), where $V(\mathbf{x}) = \frac{1}{2}(x^2 + y^2)$ and $\mu = 8$.

first excited-state/symmetry-breaking solutions. All computations were executed on a Core 2 Quad computer using MATLAB. The accuracy tolerance for the Newton corrector is 10^{-9}.

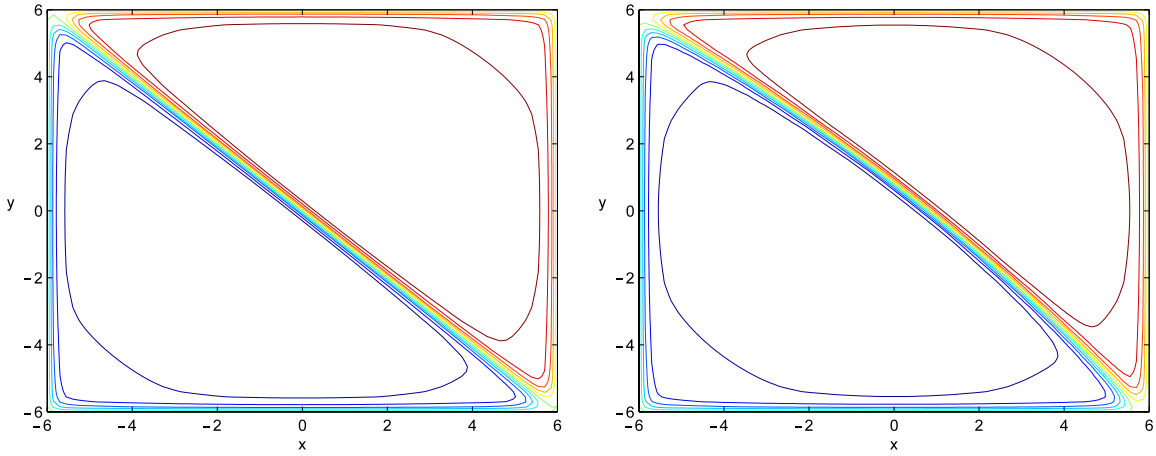

(a) The primary solution branch, where $\lambda^* \approx 2.8248$. (b) The secondary solution branch, where $\lambda^* \approx 34.5246$.

Fig. 3. The contours of the primary and secondary triangular solution curves associated with the first excited-state solution of (5.1), where $V(\mathbf{x}) = \frac{1}{2}(x^2 + y^2)$ and $\mu = 8$.

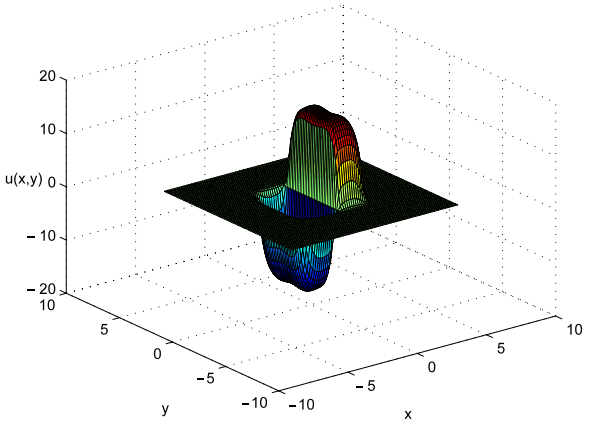

Fig. 4. The contour of the primary solution branch associated with the first excited-state solution of (5.1), where $V(\mathbf{x}) = 10(x^4 + y^4) - 20(x^2 + y^2)$, $\mu = 1$, and $\lambda^* \approx -8.6766$.

Example 1 (*Parabolic Trapping Potential*)**.** The NLS

$$\begin{aligned} &-\Delta u - \lambda u + Vu + \mu|u|^2 u = 0 \quad \text{in } \Omega = (-6, 6)^2, \\ &u = 0 \quad \text{on } \partial\Omega \end{aligned} \tag{5.1}$$

was discretized using the centered difference approximations with the uniform meshsize $h = 0.15$ on the x-and y-axis, where $V(\mathbf{x}) = \frac{1}{2}(x^2 + y^2)$ and $\mu = 8$. The first four secondary bifurcations on the second solution branch of (5.1) bifurcating at the double bifurcation $(0, \lambda_{1,2}) \approx (0, 2.8248)$ were detected at the parameter intervals (30.85, 30.88), (38.92, 38.94), (43.64, 44.02), and (48.25, 48.28), respectively. Here the number of negative eigenvalues of $D_y H$ jumps consecutively from 1 to 5. Fig. 2(a)–(b) show the primary and first four secondary solution branches associated with the first excited-state solution of (5.1). Fig. 2(c)–(f) show the contours of the first four symmetry-breaking solutions, where the nodal lines of the first excited-state solution have been twisted once, twice near the center of the domain, and so on.

Next, we investigated symmetry-breaking solutions associated with the triangular solution branches of (5.1). The first secondary bifurcation was detected at $\lambda \in (34.49, 34.58)$ on the first excited-state solution branch bifurcating at $(0, \lambda_{1,2}) \approx (0, 2.8248)$. Fig. 3(a)–(b) show the contours of the primary and secondary triangular solution curves.

Example 2 (*Quadruple-well Trapping Potential*)**.** We replaced the parabolic trapping potential in Example 1 by the quadruple-well trapping potential $V(\mathbf{x}) = 10(x^4 + y^4) - 20(x^2 + y^2)$, where we chose $\mu = 1$. The first four secondary bifurcations on the second solution branch bifurcating at $(0, \lambda_{1,2}) \approx (0, -8.6766)$ were detected at the parameter intervals (41.59, 41.71), (56.16, 56.25), (66.42, 66.44), and (77.17, 77.19), respectively, where the number of negative eigenvalues of $D_y H$ jumps consecutively from 1 to 5. The contour of the primary solution branch associated with the first excited-state solution

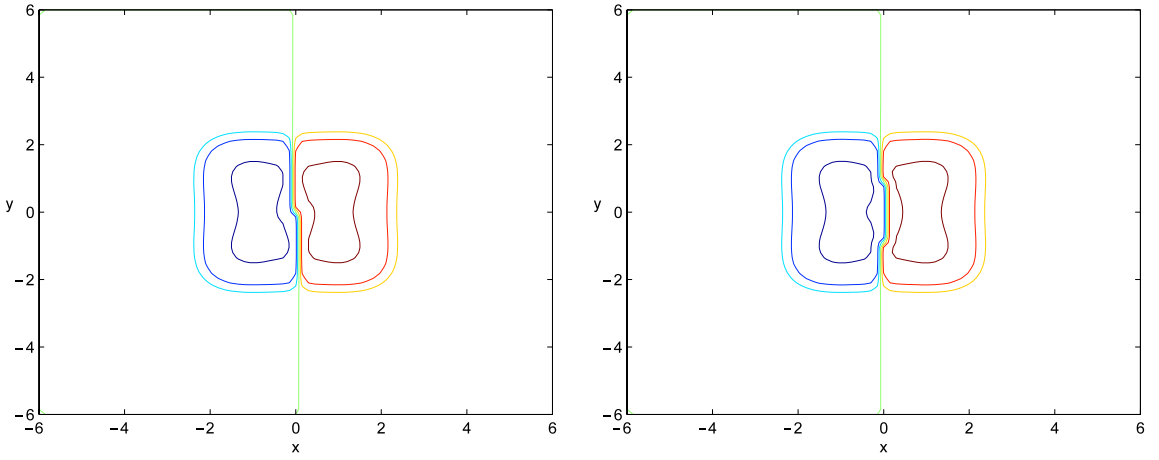

(a) The first secondary solution branch, where $\lambda^* \approx 41.6001$.

(b) The second secondary solution branch, where $\lambda^* \approx 56.2486$.

(c) The third secondary solution branch, where $\lambda^* \approx 66.4364$.

(d) The fourth secondary solution branch, where $\lambda^* \approx 77.1835$.

Fig. 5. The contours of the first four secondary solution branches associated with the first excited-state solution of (5.1), where $V(\mathbf{x}) = 10(x^4 + y^4) - 20(x^2 + y^2)$ and $\mu = 1$.

is shown in Fig. 4. Fig. 5(a)–(d) display the contours of the first four symmetry-breaking solutions associated with the first excited-state solution of the GPE. Note that the nodal line of the first excited-state has been twisted consecutively.

Next, we investigated symmetry-breaking solutions associated with the triangular solution branches. The first secondary bifurcation was detected at $\lambda \in (64.86, 64.88)$ on the first excited-state solution branch bifurcating at $(0, \lambda_{1,2}) \approx (0, -8.6766)$. Fig. 6(a)–(b) show the contours of the primary and secondary triangular solution curves.

Table 1 lists some implementation details using Algorithm 3.1 for Examples 1 and 2.

Example 3 (*Periodic Potential (Cosine Function)*)**.** The GPE

$$\begin{aligned} &-\Delta u - \lambda u + \left[V(\mathbf{x}) + a\cos^2\left(\frac{\pi x}{d}\right) + b\cos^2\left(\frac{\pi y}{d}\right)\right]u + \mu|u|^2u = 0 \quad \text{in } \Omega = (-6, 6)^2, \\ &u = 0 \quad \text{on } \partial\Omega \end{aligned} \tag{5.2}$$

was discretized using the centered difference approximations with the uniform meshsize $h = 0.15$ on the x-and y-axis, where $V(\mathbf{x}) = \frac{1}{2}(x^2 + y^2)$, $\mu = 8$, $a = b = 5000$, and $d = 1$. The first secondary bifurcation was detected at $\lambda \in (16.2389, 16.2423)$ on the first excited-state solution branch bifurcating at $(0, \lambda_{1,2}) \approx (0, 16.2372)$. The contours of the primary and secondary solution curves are shown in Fig. 7(a)–(b).

Example 4 (*Periodic Potential (Sine Function)*)**.** Consider the GPE

$$\begin{aligned} &-\Delta u - \lambda u + \left[V(\mathbf{x}) + a\sin^2\left(\frac{\pi x}{d}\right) + b\sin^2\left(\frac{\pi y}{d}\right)\right]u + \mu|u|^2u = 0 \quad \text{in } \Omega = (-6, 6)^2, \\ &u = 0 \quad \text{on } \partial\Omega. \end{aligned} \tag{5.3}$$

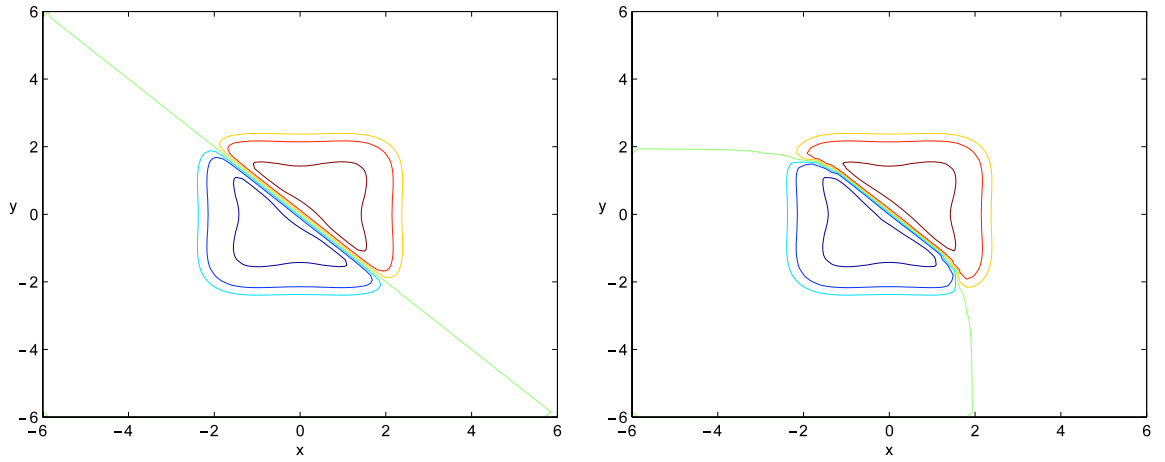

(a) The primary solution branch, where $\lambda^* \approx -8.6766$. (b) The secondary solution branch, where $\lambda^* \approx 64.8703$.

Fig. 6. The contours of the primary and secondary triangular solution curves associated with the first excited-state solution of (5.1), where $V(\mathbf{x}) = 10(x^4 + y^4) - 20(x^2 + y^2)$ and $\mu = 1$.

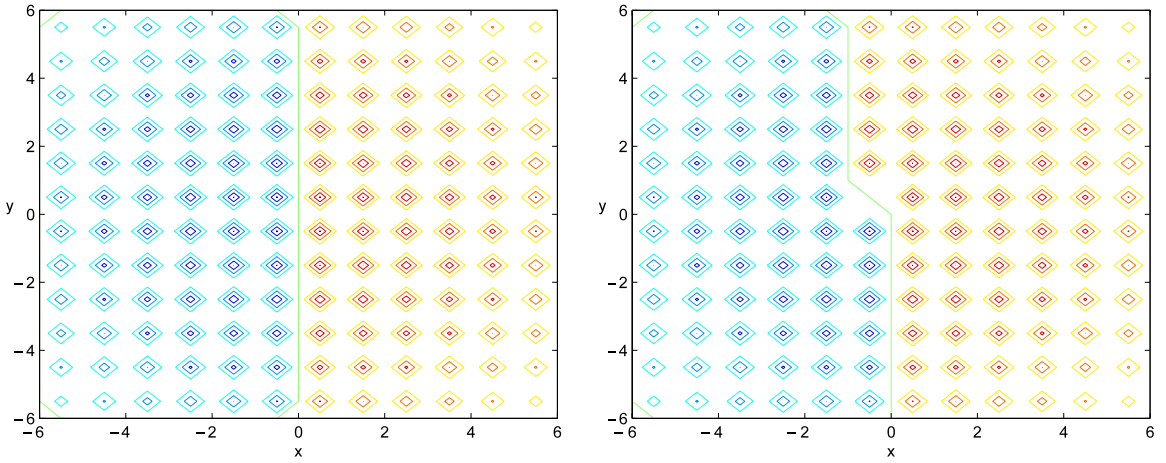

(a) The primary solution branch, where $\lambda^* \approx 16.2372$. (b) The secondary solution branch, where $\lambda^* \approx 16.2402$.

Fig. 7. The contours of the primary and secondary solution curves associated with the first excited-state solution of (5.2).

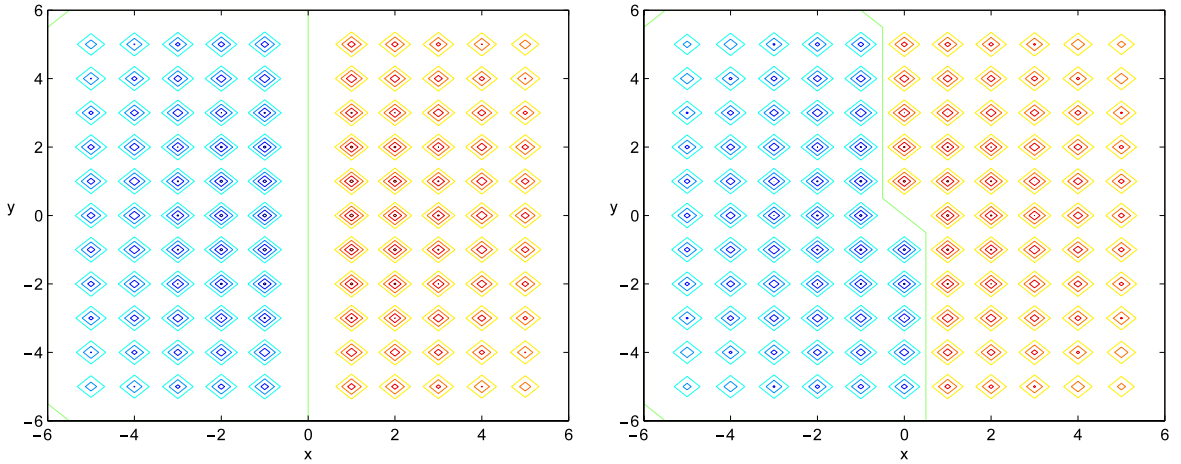

(a) The primary solution branch, where $\lambda^* \approx 16.4871$. (b) The secondary solution branch, where $\lambda^* \approx 16.48722$.

Fig. 8. The contours of the primary and secondary solution curves associated with the first excited-state solution of (5.3).

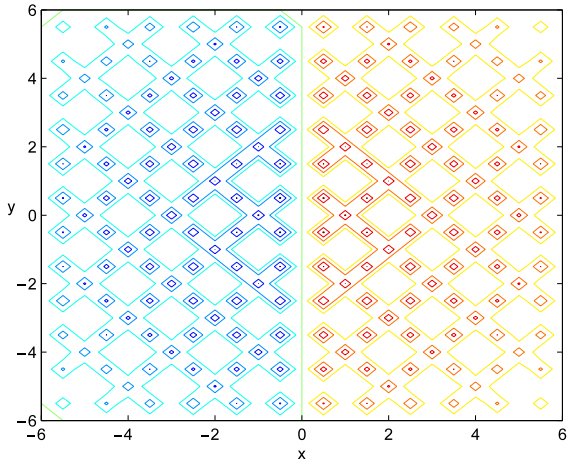

(a) The primary solution branch, where $\lambda^* \approx 16.2369$.

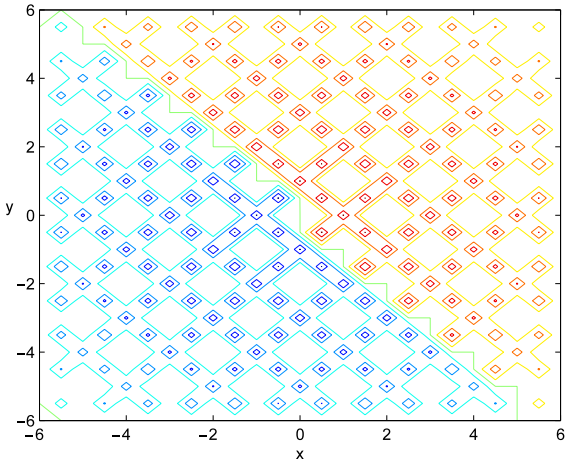

(b) The secondary solution branch, where $\lambda^* \approx 16.4867$.

Fig. 9. The contours of the primary and secondary solution curves associated with the first excited-state solution of (5.4), where $\phi = 0$.

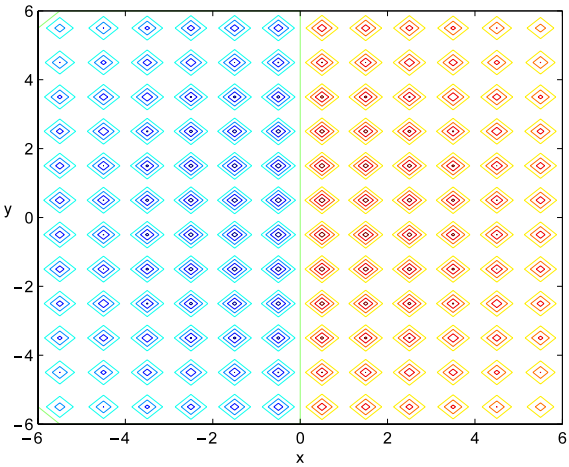

(a) The primary solution branch, where $\lambda^* \approx 16.2372$.

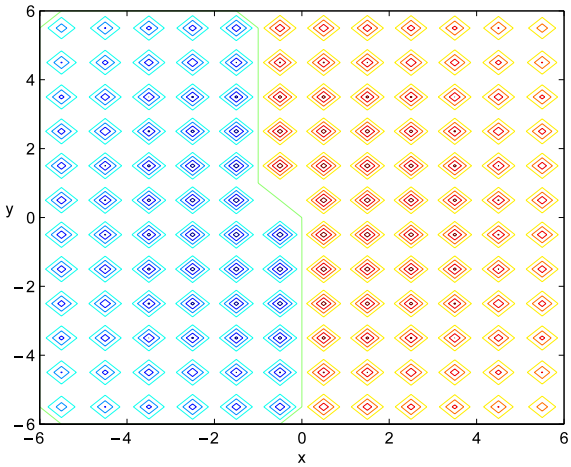

(b) The secondary solution branch, where $\lambda^* \approx 16.2402$.

Fig. 10. The contours of the primary and secondary solution curves associated with the first excited-state solution of (5.4), where $\phi = \frac{\pi}{4}$.

Table 1
Using a single grid continuation algorithm and two-grid continuation algorithm to compute the symmetry-breaking solutions of (5.1).

(a) Parabolic trapping potential $\left(V(\mathbf{x}) = \frac{1}{2}(x^2 + y^2)\right)$		
	Continuation steps	
	Coarse grid	Fine grid
A single grid with $h = 12/80$	0	133
Two-grid with $\tilde{h} = 12/40$ and $h = 12/80$ (Method (I))	86	61
Two-grid with $\tilde{h} = 12/40$ and $h = 12/80$ (Method (II))	86	60
(b) Quadruple-well trapping potential $\left(V(\mathbf{x}) = 10(x^4 + y^4) - 20(x^2 + y^2)\right)$		
	Continuation steps	
	Coarse grid	Fine grid
A single grid with $h = 12/80$	0	197
Two-grid with $\tilde{h} = 12/40$ and $h = 12/80$ (Method (I))	70	42
Two-grid with $\tilde{h} = 12/40$ and $h = 12/80$ (Method (II))	70	41

Using the same data as in Example 3, the first secondary bifurcation was detected at $\lambda \in (16.48719, 16.48725)$ on the first excited-state solution branch bifurcating at $(0, \lambda_{1,2}) \approx (0, 16.4871)$. The contours of the primary and secondary solution curves are shown in Fig. 8(a)–(b).

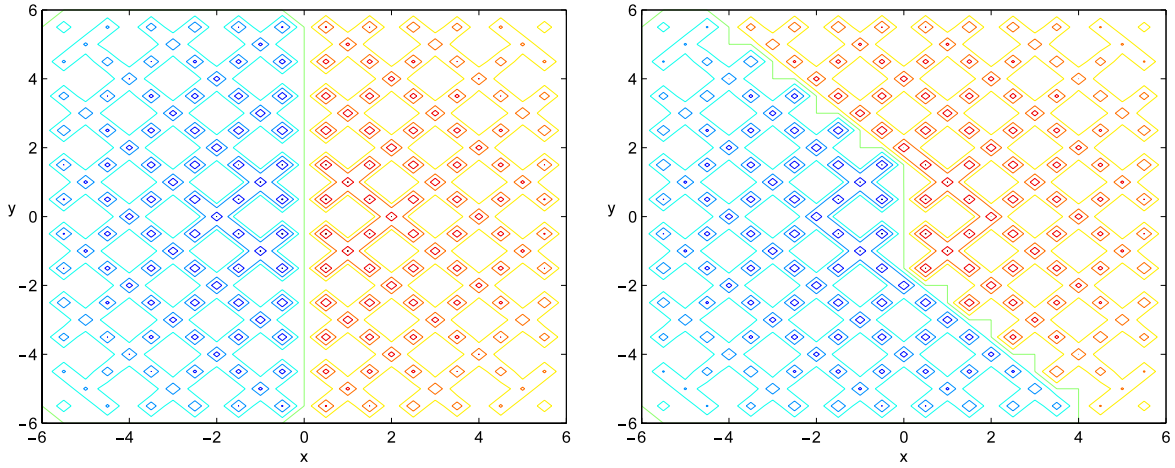

(a) The primary solution branch, where $\lambda^* \approx 16.2314$.

(b) The secondary solution branch, where $\lambda^* \approx 17.9869$.

Fig. 11. The contours of the primary and secondary solution curves associated with the first excited-state solution of (5.4), where $\phi = \pi$.

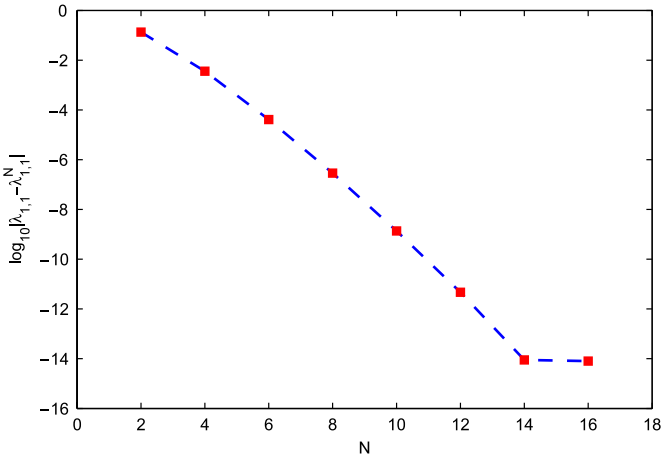

Fig. 12. The absolute errors for the spectral-Galerkin method applied to (5.5), where $\lambda_{1,1} = 2\pi^2/4 = 4.934802200544679$.

Example 5. The GPE

$$\begin{aligned} &-\Delta u - \lambda u + \left\{ V(\mathbf{x}) + a\left[\cos^2\left(\frac{\pi x}{d}\right) + \cos^2\left(\frac{\pi y}{d}\right) + 2\cos\left(\frac{\pi x}{d}\right)\cos\left(\frac{\pi y}{d}\right)\cos(\phi)\right]\right\} u \\ &\quad + \mu|u|^2 u = 0 \quad \text{in } \Omega = (-6, 6)^2, \\ &u = 0 \quad \text{on } \partial\Omega \end{aligned} \tag{5.4}$$

was discretized using the centered difference approximations with the uniform meshsize $h = 0.15$ on the x-and y-axis, where $V(\mathbf{x}) = \frac{1}{2}(x^2 + y^2)$, $\mu = 8$, $a = 5000$, $d = 1$, and $\phi = 0$, $\frac{\pi}{4}$, and π. Figs. 9–11 show the contours of the primary and secondary solution curves associated with the first excited-state solutions where $\phi = 0$, $\frac{\pi}{4}$, and π, respectively. Note that this example is the same as Example 3 if $\phi = \frac{\pi}{2}$.

Example 6. The eigenpairs of the linear eigenvalue problem

$$\begin{aligned} &-\Delta u = \lambda u \quad \text{in } \Omega = (-1, 1)^2, \\ &u = 0 \quad \text{on } \partial\Omega \end{aligned} \tag{5.5}$$

are

$$\lambda_{m,n} = \frac{(m^2 + n^2)\pi^2}{4},$$

$$u_{m,n}(x, y) = \sin\left(\frac{m\pi(x+1)}{2}\right)\sin\left(\frac{n\pi(y+1)}{2}\right), \quad m, n = 1, 2, \ldots.$$

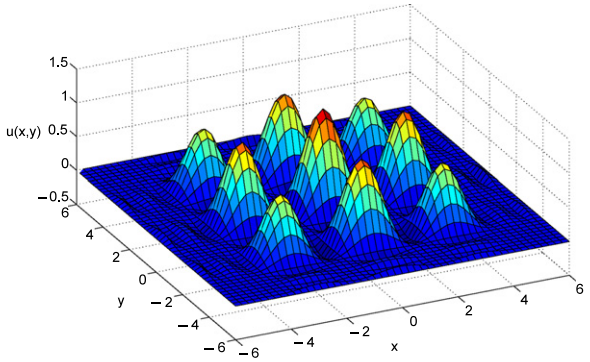

(a) The ground-state solution curve with $d = 3$.

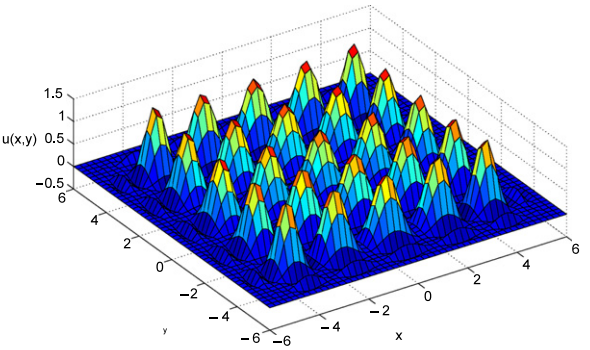

(b) The ground-state solution curve with $d = 2$.

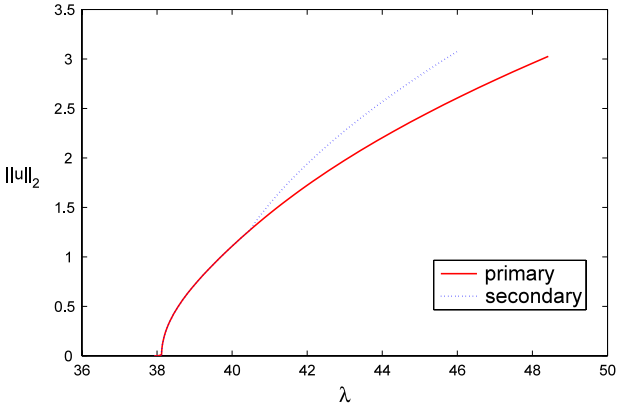

(c) Solution curves with $d = 3$.

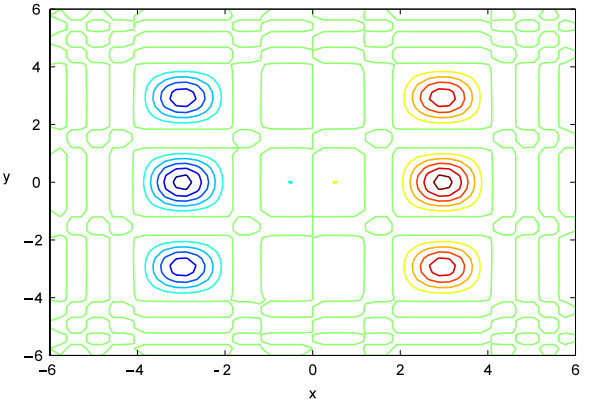

(d) The primary solution branch with $d = 3$, where $\lambda^* \approx 38.1221$.

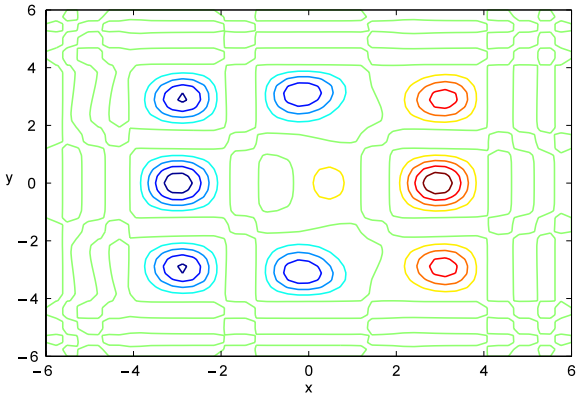

(e) The secondary solution branch with $d = 3$, where $\lambda^* \approx 40.4605$.

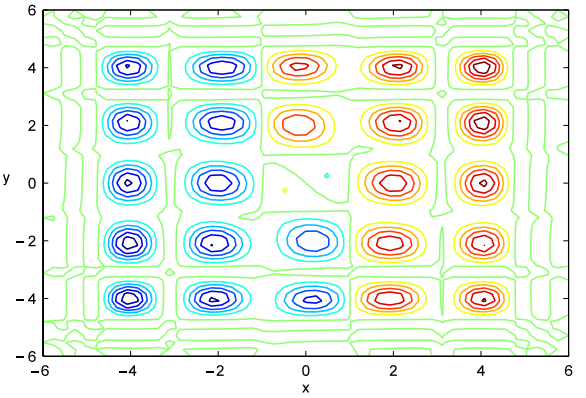

(f) The secondary solution branch with $d = 2$, where $\lambda^* \approx 53.6781$.

Fig. 13. The primary and secondary solution curves, and contours of the ground state solution curve and solution branches associated with the first excited-state solution of (5.3), where $\mu = 8$, $a = b = 100$, $d = 3$ and 2.

We used the spectral-Galerkin method described in Section 4 with $N = 20$ to discretize (5.5). Table 2 lists the first eight approximate eigenvalues of (5.5). Fig. 12 shows how the errors of the spectral-Galerkin method decrease with respect to N, which also shows that the convergence rate is exponential.

Example 7 (*Using the Spectral-Galerkin Method to Discretize the GPE*)**.** We exploited the spectral-Galerkin method described in Section 4 to discretize (5.3), where $V(\mathbf{x}) = \frac{1}{2}(x^2+y^2)$, $\mu = 8, a = b = 100$, $d = 3$ and 2. Fig. 13(a)–(b) show the contours of the ground state solution curves. The number of peaks agree with the formula $\prod_{j=1}^{2}(12/d-1)$ in [35]. Fig. 13(c) shows how the first excited-state solution bifurcating at $(\|u\|_2, \lambda_{1,2}) \approx (0, 38.1221)$, and the first secondary solution branch bifurcating at $(\|u\|_2, \lambda^*) \approx (1.2649, 40.4605)$. Fig. 13(d)–(e) display the contours of the primary and secondary solution curves associated with the first excited-state solution with $d = 3$. Fig. 13(f) displays the contour of the secondary solution curve

Table 2
The first eight approximate eigenvalues of (5.5). The notation $[\pm n]$ stands for multiplication by $10^{\pm n}$.

	Exact eigenvalue	Spectral-Galerkin method ($N = 20$)	Error
1	$\lambda_{1,1} = 4.934802200544679$	4.934802200544671	7.99[−15]
2	$\lambda_{1,2} = 12.337005501361698$	12.337005501361704	5.99[−15]
3	$\lambda_{2,1} = 12.337005501361698$	12.337005501361723	2.49[−14]
4	$\lambda_{2,2} = 19.739208802178717$	19.739208802178691	2.59[−14]
5	$\lambda_{1,3} = 24.674011002723397$	24.674011002721347	2.05[−12]
6	$\lambda_{3,1} = 24.674011002723397$	24.674011002721389	2.01[−12]
7	$\lambda_{2,3} = 32.076214303540416$	32.076214303538443	1.97[−12]
8	$\lambda_{3,2} = 32.076214303540416$	32.076214303538478	1.94[−12]

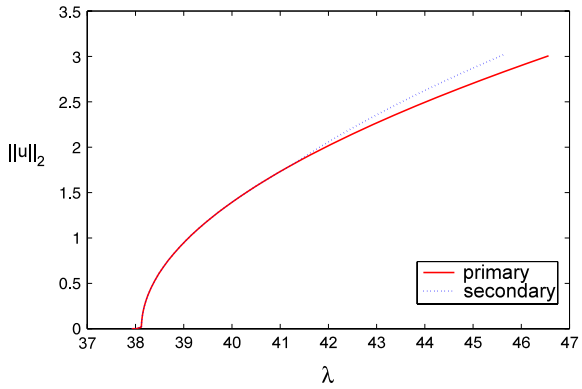

(a) Solution curves.

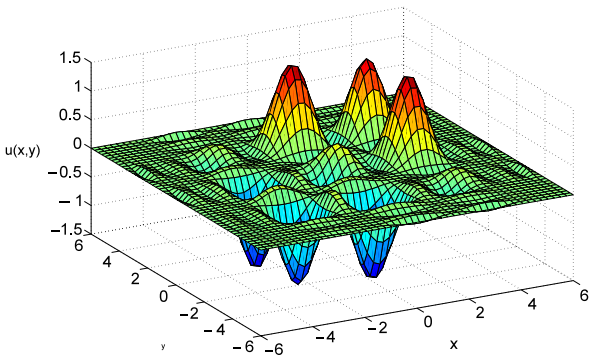

(b) The primary triangular solution branch, where $\lambda^* \approx 38.1221$.

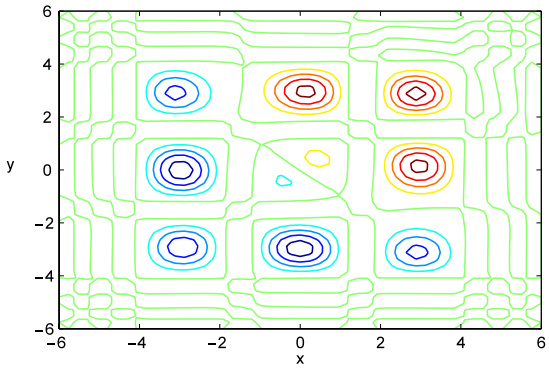

(c) The secondary triangular solution branch, where $\lambda^* \approx 41.2292$.

Fig. 14. The triangular solution branch and the first secondary solution branch, and contours of the solution branches associated with the first excited-state solution of (5.3), where $\mu = 8$, $a = b = 100$, and $d = 3$.

associated with the first excited-state solution with $d = 2$. Fig. 14(a) shows how the triangular solution branches bifurcating at $(\|u\|_2, \lambda_{1,2}) \approx (0, 38.1221)$, and the first secondary solution branch bifurcating at $(\|u\|_2, \lambda^*) \approx (1.7941, 41.2292)$. Fig. 14(b)–(d) display the contours of the primary triangular solution and the first symmetry-breaking solution.

6. Conclusions

We have proposed an efficient spectral-Galerkin continuation method (SGCM) using the second kind Chebyshev polynomials for the numerical solutions of the GPE. Some basic formulae are derived so that the eigenvalues of the associated SEP can be easily computed. Thus certain amounts of computational cost can be saved when implementing the SGCM for computing the ground state, the first excited-state as well as symmetry-breaking solutions of the GPE. We have also described a two-grid centered difference algorithm for computing symmetry-breaking solutions of the GPE. However, the latter is more expensive than the SGCM because the target point is far away from the bifurcation point, and more continuation steps are required for the curve-tracking. In addition, the two-grid scheme is not as accurate as the SGCM.

Our numerical results show that symmetry-breaking solutions exist for the following types of GPE:

(i) the GPE with parabolic trapping potential,
(ii) the GPE with quadruple-well trapping potential,
(iii) the GPE in optical lattices, where the periodic potential is described by the Fourier sine or cosine function.

Recently, we have studied spectral collocation methods [36,37] for the ground state and first excited-state solutions of a rotating BEC, and a rotating BEC in optical lattices, where the Fourier sine functions and Chebyshev polynomials were used as the basis functions. The numerical results show that using these basis functions can obtain more vortices than the centered difference method [25] and the CNGF [38]. Finally, the numerical results in [36] show that the SGCM is at least as competitive as the AITEMs. And in some examples it even outperforms the AITEMs.

Acknowledgement

The second author was supported by the National Science Council of ROC (Taiwan) through Project NSC 98-2115-M-231-001-MY3.

References

[1] J.P. Boyd, Chebyshev and Fourier Spectral Methods, Dover, Mineola, New York, 2001.
[2] D. Gottlieb, S.A. Orszag, Numerical Analysis of Spectral Methods: Theory and Applications, SIAM, Philadelphia, 1977.
[3] L.N. Trefethen, Spectral Methods in Matlab, SIAM, Philadelphia, 2000.
[4] J.C. Mason, D.C. Handscomb, Chebyshev Polynomials, Chapman & Hall/CRC, New York, 2003.
[5] J. Shen, Efficient spectral-Galerkin method II. Direct solvers of second and fourth order equations by using Chebyshev polynomials, SIAM J. Sci. Comput. 16 (1995) 74–87.
[6] R. Baer, Accurate and efficient evolution of nonlinear Schrödinger equations, Phys. Rev. A 62 (2000) 063810.
[7] S. Burger, F.S. Cataliotti, C. Fort, F. Minardi, M. Inguscio, M.L. Chiofalo, M.P. Tosi, Superfluid and dissipative dynamics of a Bose–Einstein condensate in a periodic potential, Phys. Rev. Lett. 86 (2001) 4447–4450.
[8] M. Cristiani, O. Morsch, J.H. Muller, D. Ciampini, E. Arimondo, Experimental properties of Bose–Einstein condensates in one-dimensional optical lattices: bloch oscillations, Landau–Zener tunneling, and mean-field effects, Phys. Rev. A 65 (2002) 063612.
[9] L. Fallani, F.S. Cataliotti, J. Catani, C. Fort, M. Modugno, M. Zawada, M. Inguscio, Optically induced lensing effect on a Bose–Einstein condensate expanding in a moving lattice, Phys. Rev. Lett. 91 (2003) 24045.
[10] R. D'Agosta, C. Presilla, States without a linear counterpart in Bose–Einstein condensates, Phys. Rev. A 65 (2002) 043609.
[11] W. Bao, D. Jaksch, P.A. Markowich, Numerical solution of the Gross–Pitaevskii equation for Bose–Einstein condensation, J. Comput. Phys. 187 (2003) 318–342.
[12] W. Bao, S. Jin, P.A. Markowich, On time splitting spectral approximations for the Schrödinger equation in the semiclassical regime, J. Comput. Phys. 175 (2002) 487–524.
[13] W. Bao, S. Jin, P.A. Markowich, Numerical study of time-splitting spectral discretizations of nonlinear Schrödinger equations in the semiclassical regimes, SIAM J. Sci. Comput. 25 (2003) 27–64.
[14] J.J. García-Ripoll, V.M. Pérez-García, Optimizing Schrödinger functionals using Sobolev gradients: Applications to quantum mechanics and nonlinear optics, SIAM J. Sci. Comput. 23 (2001) 1316–1334.
[15] L.-C. Crasovan, V. Vekslerchik, V.M. Pérez-García, J.P. Torres, D. Mihalache, L. Torner, Stable vortex dipoles in nonrotating Bose–Einstein condensates, Phys. Rev. A 68 (2003) 063609.
[16] L.-C. Crasovan, V.M. Pérez-García, I. Danaila, D. Mihalache, L. Torner, Three-dimensional parallel vortex rings in Bose–Einstein condensates, Phys. Rev. A 70 (2004) 033605.
[17] W. Bao, Q. Du, Computing the ground state solution of Bose–Einstein condensates by a normalized gradient flow, SIAM J. Sci. Comput. 25 (2004) 1674–1697.
[18] J. Yang, T.I. Lakoba, Accelerated imaginary-time evolution methods for the computation of solitary waves, Stud. Appl. Math. 120 (2008) 265–292.
[19] P. Muruganandam, S.K. Adhikari, Bose–Einstein condensation dynamics in three dimensions by pseudospectral and finite-difference methods, J. Phys. B 36 (2003) 2501–2514.
[20] H.Q. Wang, Numerical studies on the split-step finite difference method for nonlinear Schrödinger equations, Appl. Math. Comput. 170 (2005) 17–35.
[21] J.C. Eilbeck, P.S. Lomdahl, A.C. Scott, The discrete self-trapping equation, Physica D 16 (1985) 318–338.
[22] G.L. Alfimov, D.A. Zezyulin, Nonlinear modes for the Gross–Pitaevskii equation—a demonstrative computation approach, Nonlinearity 20 (2007) 2075–2092.
[23] S.-L. Chang, C.-S. Chien, B.-W. Jeng, Liapunov–Schmidt reduction and continuation for nonlinear Schrödinger equations, SIAM J. Sci. Comput. 29 (2007) 729–755.
[24] S.-L. Chang, C.-S. Chien, B.-W. Jeng, Computing wave functions of nonlinear Schrödinger equations: a time-independent approach, J. Comput. Phys. 226 (2007) 104–130.
[25] S.-L. Chang, C.-S. Chien, Adaptive continuation algorithms for computing energy levels of rotating Bose–Einstein condensates, Comput. Phys. Comm. 177 (2007) 707–719.
[26] V.M. Pérez-García, X.-Y. Lin, Numerical methods for the simulation of trapped nonlinear Schrödinger system, Appl. Math. Comput. 144 (2003) 215–235.
[27] E.L. Allgower, K. Böhmer, Z. Mei, A complete bifurcation scenario for the 2-D nonlinear Laplacian with Neumann boundary conditions on the unit square, in: Internat. Ser. Numer. Math., vol. 97, Birkhäuser, Basel, 1991.
[28] P.J. Budden, J. Norbury, Solution branches for nonlinear equilibrium problem-bifurcation and domain perturbation, IMA J. Appl. Math. 28 (1982) 109–129.
[29] P.L. Lions, On the existence of positive solutions of semilinear elliptic equations, SIAM Rev. 24 (1982) 441–467.
[30] C.-S. Chien, S.-Y. Gong, Z. Mei, Mode jumping in the von Kármán equations, SIAM J. Sci. Comput. 22 (2000) 1354–1385.
[31] M. Golubitsky, D.G. Schaeffer, Singularities and Groups in Bifurcation Theory, Springer-Verlag, Heidelberg, 1985.
[32] E. Isaacson, H.B. Keller, Analysis of Numerical Methods, John Wiley & Sons, New York, 1966.
[33] C.-S. Chien, B.-W. Jeng, A two-grid discretization scheme for semilinear elliptic eigenvalue problems, SIAM J. Sci. Comput. 27 (2006) 1287–1304.
[34] D.S. Bernstein, Matrix Mathematics, Princeton University Press, New Jersey, 2005.
[35] H.-S. Chen, C.-S. Chien, Multilevel spectral-Galerkin and continuation methods for nonlinear Schrödinger equatios, SIAM J. Multiscale Model. Simul. 8 (2009) 370–392.
[36] H.-S. Chen, S.-L. Chang, C.-S. Chien, Spectral collocation methods using sine functions for a rotating Bose–Einstein condensation in optical lattices, J. Comput. Phys. (submitted for publication).
[37] Y.-S. Wang, C.-S. Chien, A spectral-collocation continuation method for rotating two-component Bose–Einstein condensation in optical lattices (in press).
[38] W. Bao, H. Wang, P.A. Markowich, Ground, symmetric and central vortex states in rotating Bose–Einstein condensates, Commun. Math. Sci. 3 (2005) 57–88.